Hydrodeoxygenation of m-cresol over Pd/Al-SBA-15 catalysts: effect of Al content on the deoxygenation reaction pathways

Camila A. Teles[1,*], Carmen Ciotonea[2], Nicolas. Gomes[3], Vinicius O. O. Gonçalves[3], Adrian Ungureanu[4], Cezar Catrinescu[4], Maya Marinova[5], Jean-Marc Clacens[1], Sébastien Royer[6], Fábio B. Noronha[6,7,8], Frédéric Richard[1,*]

[1] *Université de Poitiers, CNRS, Institut de Chimie des Milieux et Matériaux de Poitiers, UMR 7285, rue Michel Brunet, BP633, 86022 Poitiers, France.*

[2] *Université du Littoral Côte d'Opale, Unité de Chimie Environnementale et Intéractions sur le Vivant-UCEIV, UR4492, SFR Condorcet FR CNRS 3417, 59140 Dunkerque, France.*

[3] *Universidade Federal do Rio de Janeiro, Instituto de Química, Departamento de Físico-Química, Av. Athos da Silveira Ramos, 149, 21949-900, Rio de Janeiro, Brazil.*

[4] *"Gheorghe Asachi" Technical University of Iasi, Faculty of Chemical Engineering and Environmental Protection"Cristofor Simionescu", 73 D. Mangeron Blvd 700050 Iasi, Romania.*

[5] *Univ. Lille, CNRS, INRA, Centrale Lille, Univ. Artois, FR 2638 – IMEC – Institut Michel-Eugène Chevreul, 59000 Lille, France.*

[6] *Université de Lille, CNRS, Centrale Lille, Univ. Artois, UMR 8181 – UCCS – Unité de Catalyse et Chimie du Solide, F-59000 Lille, France.*

[7] *National Institute of Technology, Catalysis Division, Av. Venezuela 82, Rio de Janeiro, 20081-312, Brazil.*

[8] *Military Institute of Engineering, Chemical Engineering Department, Praça Gal. Tiburcio 80, 22290-270, Rio de Janeiro, Brazil.*

* Corresponding author: frederic.richard@univ-poitiers.fr; camilaabreuteles@gmail.com

Submitted to Apply Catalysis A: General

March 2022

Abstract

The effect of aluminium content (x = 5, 20 and 40 wt.%) in SBA-15 type silica supports used to obtain Pd/xAl-SBA-15 catalysts was evaluated in the HDO reaction of m-cresol at 300 °C, under atmospheric and high (30 bar) pressure. Aluminium incorporation was performed using the two-step pH-adjustment method, affording the deposition of Al phases over silica previously precipitated. Pd was thereafter deposed using incipient wetness impregnation. Physico-chemical properties of the catalysts were investigated by XRD, N_2 physisorption, H_2 chemisorption, DRIFTS of adsorbed pyridine, STEM-EDX mapping coupled to HAADF imaging. The acidity (Brønsted and Lewis sites) generated by the incorporation of aluminium at low content (i.e. 5 wt.%) onto the SBA-15 structure resulted in the improvement of HDO of m-cresol, with an increase in selectivity toward the deoxygenated products, toluene under atmospheric pressure (38% for the Pd/SBA vs. 77% for the Pd/Al5-SBA) and methylcyclohexane under high pressure (14% for the Pd/SBA vs. 30% for Pd/Al5-SBA). The selectivity into methylcyclohexanone was also affected by the total pressure: 5% under atmospheric pressure vs 64% under 30 bar over Pd/Al5-SBA). However, under atmospheric pressure, at higher Al contents, side reactions catalyzed by acid sites were promoted, such as isomerization and disproportionation reactions, which were not observed under high pressure. Besides that, the increase of quantity of Al leaded to the decrease of the surface accessibility and hence drop on the reactions rate over both pressure conditions. This work demonstrated the efficiency of Pd catalyst in HDO reaction which can be obtained by a precise adjustment of the quantity of Al in the SBA catalytic support.

Keywords: HDO; m-cresol; palladium, SBA-15, aluminium, acidity.

1. Introduction

The production of biomass-based bio-oil from pyrolysis of lignocellulosic feedstock, has attracted significant interest during the last decade. However, the large-scale use of this bio-oil is restricted due its high oxygen content that leads to undesirable characteristics, such as low energy density, thermal and chemical instability [1,2]. Hydrodeoxygenation (HDO) process is intensively studied [3-5] since it is efficient to remove oxygen atoms, while preserving the carbon number of hydrocarbons chain, thus allowing the production of higher heating value fuels. Being a complex reaction giving numerous products, heterogeneous catalysts help to orientate the reaction toward the obtention of valuable deoxygenated molecules [6,7].

Considering the high complexity composition of the bio-oil, representative model molecules, such as phenolic compounds (phenol, m-cresol, anisole and guaiacol), are often used in order to study catalytic HDO [8-19]. So far, three main reaction pathways have been proposed for the HDO reaction of phenolic compounds, such as m-cresol: (i) hydrogenation (HYD) of the aromatic ring, to produce an alcohol which dehydrates to alkene in the presence of acid sites [8-10]; (ii) direct deoxygenation (DDO) with cleavage of the C-O bond, yielding aromatics [11-14]; and (iii) tautomerization, producing an intermediate keto tautomer, which further hydrogenates to produce (3-methyl)-cyclohexanone and (3-methyl)-cyclohexanol (ring hydrogenation), or unsaturated alcohols (hydrogenation of C=O bond) which dehydrated to toluene [11,14-19]. As evidence, the catalyst, through its metallic composition and surface acidic characteristics and the reaction conditions (temperature, pressure, contact time), will play an important role in the HDO reaction controlling the rates in the different reaction pathways.

Several catalyst formulations have been investigated for the HDO of phenolic compounds. Metals, such as: Pt, Pd, Rh, Ru, Re, Ni, and Co, combined with different supports, including SiO_2, Al_2O_3, CeO_2, ZrO_2, TiO_2, Nb_2O_5, MoO_3, V_2O_5, C, HY, Beta, and ZSM-5 zeolites were

reported [8-28]. It was demonstrated that the product selectivity and reaction mechanism are strongly dependent of the catalyst nature. Noble metals, such as Pt, Pd and Rh as well as Ni and Co, supported on inert materials like silica and carbon preferentially promote the ring hydrogenation yielding oxygenated products ((methyl)-cyclohexanol and (methyl)-cyclohexanone) [8,11,25,28]. However, the same metals, when supported on acid materials, such as Al_2O_3 and zeolites, promote further dehydration of the hydrogenated intermediate products, leading to the production of alkenes ((methyl)-cyclohexene) [8,10,29]. Once the metallic phases are supported on oxophilic materials, such as ZrO_2, TiO_2, Nb_2O_5, the cations of the support bind to the oxygen atom of the phenolic compounds. Then, the direct cleavage of C-O bond by the DDO route is favored, or the keto tautomer form of phenol/m-cresol stabilizes, thus promoting the selective hydrogenation of the carbonyl bond [13-16]. Besides supports, oxophilic metals, such as Ru and Re, are also able to promote the deoxygenation degree of bio-oil, promoting the aromatics production [11,12,17,19].

Among the potential supports, mesoporous SBA-15-type silica possesses ordered two-dimensional hexagonal *p6mm* symmetric channel-type mesopores with wide pore sizes (~4-10 nm) and thick pore walls (>1 nm). Such properties allow the diffusion of large reactants, while conferring to the support sufficient thermal and hydrothermal stability for demanding reactions [30,31]. Gage et al. [32] tested intercalated Pd particles into the framework of SBA-15-type mesoporous silica in the HDO of phenol under liquid phase. The confinement of the Pd nanoparticles (NPs), at a size of 4.5 nm, onto the walls of SBA-15, prevented the metal sintering at high temperatures and the used catalyst, partially deactivated, can be regenerated almost completely, even after numerous reaction cycles. Indeed, conversion of phenol started at 95% and decreased to 43% after 5 reaction cycles. Then, catalyst was reactivated by heating in air at 800 °C for 30 min exhibiting 80% of conversion. However, under this condition, the main hydrogenated product formed at 300 °C was an alcohol (71% of cyclohexanol) since this

support is inert. Insertion of aluminium into the structure of the SBA-15 is a strategy recently employed to modify inert silica surface [33-37]. Gbadamani et al. [33] firstly tested a series of Ni supported on Al-SBA-15 modulating the acidity of the catalysis by varying the Si/Al molar ratio for the HDO reaction of bibenzofuran. While Ni/SBA-15 catalysts orientated the reaction through the formation of hydrogenated products containing oxygen (mainly cyclohexyl-cyclohexanone, hexahydro-dibenzofuran), the Al-based supports promoted the formation of deoxygenated products via dehydration reaction (60% of deoxygenated products such as bicyclohexane). Similar trend was reported by Li et al. [35] for the HDO of eugenol over comparable catalysts. Over Pt/(Al)-SBA-15 catalysts [37], HDO of anisole occurred through the ring hydrogenation over Pt while the support acid sites promote the demethoxylation of the hydrogenated intermediate, thus leading to increased selectivity towards the deoxygenated products (cyclohexane and benzene in the reaction performed at liquid phase, 200 °C and 20 Bar of H_2). These findings demonstrated that adjusting the metal/acidic functions interface on a stable catalyst structure, provides a promising strategy to produce efficient catalysts for the upgrading of the bio-oil.

In this work, we study the impact of the support acidity in palladium based catalysts for the deoxygenation of m-cresol. For this purpose, a series of Pd supported on SBA-15, functionalized with aluminium (Al = 0, 5, 20 and 40 wt.%), were prepared and tested in the HDO reaction of m-cresol at 300 °C under atmospheric pressure and under more realistic conditions, i.e. high pressure (30 bar). Systematic catalyst characterizations were performed, and their properties were correlated with the catalytic results in order to identify the role of surface acidity on the HDO reaction mechanism.

2. Experimental Section

2.1. Materials

All chemicals required to prepare the mesoporous SBA-15, aluminium silica supports and the PdO containing materials were used as purchased: $Si(OC_2H_5)_4$ (TEOS, 98 wt.%, Sigma-Aldrich), non-ionic triblock copolymer Pluronic P123 (poly(ethylene oxide)-block-poly(propylene oxide)-blockpoly(ethylene oxide)-block, $PEO_{20}PPO_{70}PEO_{20}$, molecular weight of 5800, BASF Corp. Sigma Aldrich), hydrochloric acid (HCl, 37 wt.%, Sigma-Aldrich), aluminium nitrate nonahydrate ($Al(NO_3)_3 \cdot 9H_2O$, 98 wt.%, Sigma-Aldrich), palladium nitrate ($Pd(NO_3)_2$, 40 wt.% Pd Sigma-Aldrich).

2.2. Support Preparation

The SBA-15 support was prepared by a conventional procedure. 4.0 g of structure directing agent (P123) were solubilized in 150 mL of 1.6 M HCl at 40 °C under stirring. The silicon source (TEOS, 8.5 g) was added dropwise, and after complete adding, the solution was maintained under stirring at 40 °C for 2 h. The resulting mixture was thermally treated for 48 h at 100 °C in a sealed recipient. The solid was recovered by filtration and washing. Drying was performed for 24 h at 100 °C. As made SBA-15 was further calcined at 550 °C for 6 h (in a muffle furnace, using a heating ramp of 1.5 °C min^{-1}) to remove the organic template [38]. The support is thereafter denoted SBA-15.

Since the direct incorporation of Al in the silica framework is not feasible due to the acidic conditions applied for the SBA-15 synthesis, Al-SBA-15 supports were prepared by two-steps pH-adjusting method [38,39]. The procedure described for the synthesis of Al-SBA-15 was applied using TEOS as silica source, which is similar with the synthesis of Al-free SBA-15 sample. Thus, after the addition of TEOS to the aqueous acidic solution of P123 surfactant, the solution was aged for 2 h under stirring, and then,

the aluminium precursor, $Al(NO_3)_3 \cdot 9H_2O$, was added, the final solution being aged during 24 h under stirring. The gel was subjected to a first hydrothermal treatment at 100 °C for 48 h. The resulting suspension was cooled down to ambient temperature. At this step, aluminium cations are not incorporating the silica framework and remain in the solution. Then, the pH value of the mixture was adjusted to 7.5 by using a 4 M ammonia solution, a pH affording the precipitation of Al^{3+} in the form of (oxy)hydroxide at the surface of the silica support previously condensed. The suspension was then subjected to a second hydrothermal treatment at 100 °C for 48 h. The final solids were recovered by filtration, washed with distilled water, and then dried at 100 °C for 12 h. Finally, solids were calcined using the same procedure than applied for SBA-15. Samples with varying alumina loadings corresponding to 5, 20 and 40 wt.% Al on SiO_2 were prepared. The calcined aluminosilicate samples were designated xAl-SBA, where x is the aluminium content in the material expressed as wt.% Al (X = 5, 20 and 40).

2.3. Catalyst Preparation

Palladium precursor, $Pd(NO_3)_2$, was introduced within the pores of supports by using incipient wetness impregnation (IWI) over calcined SBA-15 and Al-SBA-15 supports. The aqueous metal nitrate precursor solutions were prepared to obtain loadings degrees of 2 wt.% Pd, and the volume of impregnation solutions was adjusted to the pore volume of the support. After dropwise addition of the solutions to supports, the impregnates were homogenized and then, the solids were transferred to an oven and heated at 120 °C for 12h. The catalysts were finally calcined under air at 400 °C for 3 h (heating ramp of 2 °C min^{-1}) to obtain the supported PdO catalysts. The materials were denoted Pd/SBA and Pd/Alx-SBA (x is the Al content in the support), respectively.

2.4. Catalyst Characterization

Catalyst composition was determined by ICP-OES. Analyses were performed using Perkin Elmer Optima 2000 DV. Before analysis, a known amount of sample was dissolved in a diluted HF-HCl solution and heated under microwave until complete dissolution.

Textural properties of catalysts were obtained by N_2 physisorption at -196 °C. Experiments were performed on a Micromeritics Tristar II automated gas sorption system. Before analysis, the samples were outgassed under dynamic vacuum at 300 °C for 3 h. Textural properties were calculated using the Tristar II software version 1.55. Specific surface areas are calculated using the multipoint B.E.T. algorithm, in the 0.10 – 0.25 P/P_0 interval. The mesopore size distribution was calculated using the BJH equation applied to the desorption branch of the isotherms. The pore volume was determined on the adsorption branch at $P/P_0 = 0.98$.

Support porosity ordering was evaluated by small angle X-ray scattering (SAXS). Experiments were performed at room temperature on a Xeuss 2.0 (Xenocs) system operated under vacuum with a GeniX3D microsource (λ = 1.54 Å) at 0.6 mA and 50 kV, and a 2D Pilatus 3R 200K detector. The sample-to-detector distance was 1005 mm.

Crystalline phase detection was performed by X-ray diffraction (XRD), using a Bruker X-ray AXS D8 Advance diffractometer in Bragg-Brentano geometry configuration fitted with a LynxEye Super Speed detector. XRD patterns were recorded with Cu Kα radiation (λ = 0.154 nm, 40 kV, 30 mA) in the 10–80° 2θ range with a 0.02° 2θ step. Phase identification was performed by comparison with the ICDD database.

Material morphology was evaluated by scanning transmission electron microscopy (S/TEM) using high angle annular dark field (HAADF) detector. The observation was performed on a TITAN Themis 300 S/TEM instrument, with a probe aberration corrector and monochromator, allowing spatial resolution of 70 pm and energy resolution of 150 meV. The microscope is equipped with a super-X windowless 4 quadrant SDD (silicon drift detector)

detection system for the STEM-EDX (energy dispersive x-ray) mapping. The experiment has been performed with a 0.5 nm probe size, a convergence angle of 21 mrad and a probe current of approximately 100 pA. For the HAADF images collection angles were between 50 and 200 mrad. Prior to observation, samples were embedded in a polymeric Epoxy resin and cut into sections of 50 nm using an ultramicrotome equipped with a diamond knife. Cuts were deposited on carbon grids for analysis.

Palladium precursor reduction was studied by temperature-programmed reduction (H_2-TPR). Experiments were conducted on an Autochem chemisorption analyser (Micromeritics), equipped with a TCD for hydrogen consumption quantification. Before TPR run, the solid was heated under 50 mL min^{-1} of simulated air at 200 °C (heating ramp of 10 °C min^{-1}, isothermal time of 1 h). After cooling down to 25 °C, the H_2 containing flow was stabilized (50 mL min^{-1}, 5.0 vol.% H_2 in Ar) and the TPR was performed from 50 °C to 800 °C (temperature ramp of 10 °C min^{-1}).

Palladium dispersion was calculated from H_2 chemisorption data. Analysis was carried out on a Micromeritics AutoChemII instrument. After reduction under pure hydrogen at 300 °C for 1 h, the sample was purged under Ar, and H_2 pulses were sent to samples at 70 °C. Palladium dispersion was calculated using eq. (1), supposing that chemisorption results in one hydrogen atom per palladium atom:

$$D\,(\%) = \frac{2 \times P \times V_{H_2} \times m_{cata}}{10^6 \times R \times T \times n_{Pd}} \qquad (1)$$

with, P, pressure (Pa); V, volume of adsorbed H_2 (mL); R = 8.314 J K^{-1} mol^{-1}; T = 295 K; m_{cata}, sample weight (g); n_{Pd}, number of mole of palladium as quantified by ICP.

Palladium particle size (Å) was determined using eq. (2), supposing hemispherical particles formation:

$$d_{average} = \frac{6C_a PM \times 10^9}{\rho \mathrm{DN}_{\mathrm{AV}}} \quad (2)$$

with C_a, the concentration of surface metal atoms (1.27. 10^{19} atoms m^{-2}); *PM*, Pd atomic mass (106.42); ρ, Pd volumetric mass (12.02. 10^6 $g.m^{-3}$); *D* metal dispersion; N_{av}, Avogadro number.

Acidic properties of catalysts were evaluated by DRIFTS of adsorbed pyridine. Experiments were conducted on a Nicolet Nexus instrument equipped with a DTGS detector and a quartz cell with CaF_2 windows. The samples were first heated at 400 °C under vacuum for 12 h. Then, the samples were cooled down to 150 °C, and a spectrum of the sample is registered as reference. Then, pyridine adsorption was carried out during 5 min, and then a vacuum purge was performed during 1 h. Finally, spectra were recorded after heating under vacuum at 150°C. Spectra were recorded between 150 and 450 °C at a resolution of 2 cm^{-1} and accumulating 64 scans bet.

2.5. Transformation of m-cresol

The catalytic experiments were conducted in vapor-phase, using a fixed-bed reactor system, operating at 300 °C under atmospheric and high (30 bar) pressure. For the reaction conducted at atmospheric pressure, a H_2/m-cresol molar ratio of 60 was selected for the reaction. Prior to reaction, the catalysts were reduced *in situ* under pure hydrogen (30 mL min^{-1}, heating rate of 5 °C min^{-1}, 300 °C for 1 h). The liquid feedstock, composed by m-cresol (7 mol %), n-heptane (3 mol %) used as internal standard, and dodecane as solvent, was introduced at the top of the reactor by using a push-syringe.

The reaction conducted under 30 bar of total pressure was carried out over the same H_2/m-cresol molar ratio used under atmospheric pressure. Prior to reaction, the catalysts were reduced *in situ* under pure hydrogen (under 30 bar, at 300 °C during 1h). The liquid feedstock used was

the same that the one used under atmospheric pressure. In this case it was introduced using a HPLC Gilson pump.

In both cases, the bottom of the reactor was kept at 5 °C using a circulator Huber minichiller. Liquid samples were collected and analyzed by a Varian 430 chromatograph equipped with a DB-5 capillary column (length: 30 m; inside diameter: 0.25 mm, film thickness: 5 μm) and a flame-ionization detector (FID). The catalysts were tested at different contact times, which were estimated by the w/F ratio, w being the catalyst weight (in g) and F the molar flow rate of m-cresol (in mol h^{-1}). Appropriate contact times values were used to keep the m-cresol conversion lower than 10% to ensure differential conditions. Gaseous products were never observed after the stabilization of catalyst. The conversion of m-cresol and product selectivity for each product were calculated using eqs. (3) and (4):

$$\mathbf{X}\ (\mathbf{in}\ \%) = \frac{\mathbf{n^0_{m-cresol} - n_{m-cresol}}}{\mathbf{n^0_{m-cresol}}} \times \mathbf{100} \qquad (3)$$

$$\boldsymbol{S_i}\ (\mathbf{in\ mol}\ \%) = \frac{\mathbf{n_i}}{\mathbf{n^0_{m-cresol} - n_{m-cresol}}} \times \mathbf{100} \qquad (4)$$

where $n^0_{m\text{-}cresol}$ and $n_{m\text{-}cresol}$ are the number of moles of m-cresol, at the initial stage and after stabilization (obtained after 1 hour on stream), respectively; n_i is the number of moles of a given *i* product.

The total reaction rate (r_{TOT} in mmol g^{-1} h^{-1}) and the reaction rates for each pathways (r_{DDO} for deoxygenation leading to toluene, r_{HYD} for aromatic ring hydrogenation mainly leading to 3-methylcyclohexanone, r_{ISOM} for isomerization leading to o-cresol (m-cresol and p-cresol being not well separated under the chromatographic conditions used), and r_{DISP} for disproportionation leading to phenol and xylenols) were calculated considering the conversion of m-cresol and the yield of the respective products (Y_i) using eq. (5) and (6):

$$\mathbf{r_{TOT}\ (in\ mmol\ g^{-1}\ h^{-1})} = \frac{X.F}{w} \quad (5)$$

$$\mathbf{r_{y}\ (in\ mmol\ g^{-1}\ h^{-1})} = r_{TOT}.S_y \quad (6)$$

where r_{TOT} is the total reaction rate for m-cresol transformation, r_y is the reaction rate in each reaction routes (DDO, HYD, ISOM and DISP), X is the m-cresol conversion, F is the m-cresol flow rate (in mmol h^{-1}), w is catalyst weight (in g) and S_i is the selectivity of different products (toluene for DDO route, 3-methylcyclohexanone, 3-methylcylohexanol, methylcyclohexene isomers and methylcyclohexane for the HYD route, *o*-cresol for the ISOM route, phenol and xylenols for the DISP route).

For all experiments, the mass balances were always between 95 and 100%.

3. Results and Discussion

3.1. Catalyst Characterization

Elementary analysis showed that the samples presented the expected values of aluminium contents, i.e. 5, 20, and 40 ± 1 wt.% (Table 1). The Pd loadings in the catalysts are also close to the expected values of 2 wt.% (range of 1.7-2.0 wt.%).

SAXS results are presented in Fig. 1a. The SAXS patterns exhibit three main diffractions associated to the *(100), (110)* and *(200)* reflections of the ordered hexagonal pore structure of the SBA-15 materials with a *P6mm* symmetry [41]. The presence of these reflections indicates that Al introduction onto the SBA-15 structure during the pH-adjustment step, does not result in a collapse of the SBA-15 pore network, as previously demonstrated for Al-SBA-15 supports at Si/Al atomic ratio from 130 to 5.2 [38]. For Pd/SBA and Pd/Alx-SBA materials, the main reflection presents a lower intensity and a slight shift compared to the diffractogram of the SBA-15 material [41]. Such modifications originate from the difference of density between materials and give valuable indications on the localization of the loaded phase in the support mesopores [39]. Fig. 1b shows the high angle XRD patterns for the palladium oxide loaded catalysts. Reflections of 2θ at 33.9°, 43.8°, 55.4° can be indexed to the PdO phase (*(101), (110)* and *(112)* reflections (ICCD 88-2434). The low intensity and width of the reflections suggest the formation of small crystallites of PdO dispersed over the support. However, considering the raw intensity of the reflections, slightly higher for Pd/SBA and Pd/Al40, the formation of slightly larger PdO particles is expected for these two catalysts.

Textural properties of the catalysts are listed in Table 1 and the corresponding adsorption/desorption isotherms are shown in Fig. 2a. The isotherms are all type IV with H1 hysteresis loops located at P/P_0 between 0.6-0.8 which corresponds to the pore structure of SBA-15 type support possessing uniform disposition of cylindrical pores [38,39]. However, the hysteresis loop shifted to lower P/P_0 and slightly changed the shape in the presence of high

aluminum content. A preferential localization of the Al_2O_3 and PdO phase inside the mesopore can explain this evolution, as also suggested on the basis of SAXS results. Indeed, the partial filling of pores by Al_2O_3 phase may causes some obstruction, thus modifying pore distribution as measured by N_2-physisorption. In addition, the slightly elongated hysteresis shape for Al-containing materials can originate from the Al incorporation step at pH~7.5 and the further ageing [41].

The deposition of Al induces a decrease of the total surface area, from 539 $m^2 g^{-1}$ (Pd/SBA) to 377-378 $m^2 g^{-1}$ for Pd/Al5-SBA and Pd/Al20-SBA materials, and to 279 $m^2 g^{-1}$ for Pd/Al40-SBA material. This trend is associated with the possible blockage of a part of the mesopores in supports when Al content increases as well as the ~2 times higher density of alumina phase with respect of silica [38]. A decrease in the microporous surface area is observed upon Al deposition, as already reported [41,42]. A comparable evolution is observed for the pore volume, which decreases by 25% and 55 for low Al-loading Pd/Al40-SBA, respectively. The average pore size is around at ~7.1-7.3 nm for Al-free and low-loading Al catalysts, whereas the Pd/Al40-SBA material presents a slightly lower pore diameter (6.0 nm), which is coherent with the possible obstruction of a part of mesopores or pore size reduction due to silica surface covering by an alumina layer for this support at high alumina loading [38].

Information on structural ordering and pore architecture of the Alx-SBA materials, as well as the location and size of palladium oxide particles are obtained from HAADF images. STEM-EDX element mapping was used to investigate the distribution palladium oxide particles throughout the support pores. Representative HAADF images of the calcined PdO containing samples are presented in Figs. 3 and 4 and Figs. S1-S4 (ESI). The images show well-ordered arrays of mesopores regardless of the sample, even for the Pd/Al40-SBA catalyst, for which a noticeable modification of the isotherm shape is observed (Fig. 2). The STEM-EDX analysis of Al element (Fig. 4(g-i)) shows a uniform distribution of the Al element within the silica

structure whatever the loading. However, when the loading increases, STEM images of the silica grains revealed some alumina enrichment on the grain periphery (Fig. S5, ESI) show Al_2O_3 particles occluding mesopores, as well as a thick layer of Al_2O_3 accumulated at the external surface, as previously observed [40,43,44]. These phenomena explain the evolution of the textural properties of Pd/Al40-SBA, i.e. a dramatic decrease in surface area and pore volume, with decrease of average pore diameter.

For Pd/SBA and Pd/Al5-SBA, PdO nanoparticle (NP) sizes observed by microscopy are between 2 and 6 nm (Fig. 3), with an average particle size of 3.4 and 2.9 nm, respectively (Table 2). The PdO NPs are exclusively confined inside the mesopores, and agglomerated in the form of few NPs assemblies (Fig. 3 and Figs. S1-S2, ESI). Pd/Al20-SBA exhibits PdO NPs of uniform size as observed on the histogram presented in Fig. 3, leading to a smaller average particle size (2.4 nm, Table 2). However, the NPs are located both inside the mesopores and at the external surface of the grain (or pore mouth) as observed in Fig. 3 and Fig. S3 (ESI). In addition, the nanoparticles are aggregated in the pores, forming larger assemblies than for the Pd/SBA and Pd/Al5-SBA samples. For the Pd/Al40-SBA sample, PdO particles positioning both in the porosity and at the pore entrance or at the external surface.

The accumulation of PdO NPs at the periphery of the support grain can be associated to the enrichment of this zone with Al_2O_3 phase. Indeed, the isoelectric point (IEP) of Al_2O_3 (IEP = 8.7) is higher than for SiO_2 (IEP = 3.9). Palladium speciation in water at pH~2 (pH value of the impregnation solution) should favor the formation of cations, which may be stabilized and will preferentially interact with the charged surface of alumina layer. Electrostatic interaction will also lead to a better thermal stability of the PdO NPs, and consequently lower PdO sizes over highly-loaded Al-containing supports than for Pd/SBA and Pd/Al5-SBA are expected.

Metallic dispersion of palladium particles was estimated by chemisorption of H_2 after *in situ* reduction of the samples. Calculated values are presented in Table 2. Similar values of

metallic dispersion of 47 % are obtained for Pd/SBA and Pd/Al5-SBA, which reflects a limited level of dispersion, and the formation of relatively large particles (2.4 nm indicated in Table 2). Pd/Al20-SBA present a dispersion of 61%, the highest level in the series. A drop of Pd dispersion was measured for the Pd/Al40-SBA sample (38%). The formation of larger particles over Pd/SBA and Pd/Al5-SBA is not surprising, which is in line with the results obtained from XRD and TEM analyses. Also, the dispersion value for Pd/Al20-SBA was expected to be comparable with Pd/Al40-SBA which is clearly not the case. This result could however be related to the observed aggregation of Pd particles in the support pores, leading to a decrease of the surface accessibility and consequently to a drop in dispersion, without elementary particle growth.

Pyridine adsorption-desorption DRIFTS experiments are presented in Fig. 5. The total acidity and the acidic site distribution over the catalysts are listed in Table 2. No bands are observed on the spectra of Pd/SBA, indicating the absence of noticeable acidity for this catalyst. The spectra of the Pd/Alx-SBA exhibited bands associated to pyridine adsorbed on Lewis acid sites at 1456 and 1624 cm^{-1}; pyridine adsorbed on Brønsted acid sites at 1547 cm^{-1}; pyridine associated with both Lewis and Brønsted acid sites at 1490 cm^{-1} [45,46]. The total concentration of acid sites as well as the concentration of Brønsted and Lewis sites are reported in Table 2. The introduction of Al onto the silica structure allows the formation of both Lewis and Brønsted acid sites, accordingly to the literature [38,46,47]. However, the density of Brønsted acid sites remained low and constant (35 µmol g^{-1}), regardless of the aluminium content. On the contrary, the density of Lewis acid sites significantly increased with the Al content from 178 µmol g^{-1} for Pd/Al5-SBA to 240 µmol g^{-1} for Pd/Al40-SBA. Previously, Ungureanu et al [38] showed that total acidity in Al-SBA increases with Al content in the materials, as determined by pyridine adsorption. However, Bronsted to Lewis site ratio was not significantly affected by the Al loading. Then aluminium incorporation, even by two step pH

adjusting method was efficient to increase both Bronsted and Lewis sites. Lindo et al. [48] also observed the formation of Lewis acid sites over Ni/Al-SBA-15 catalysts with different content of aluminium, which were associated with the presence of extra-framework Al in octahedral coordination (Al_2O_3 phase). The Lewis acidity does not vary linearly with the aluminium content. However, when calculated per surface area unit, Lewis acidity is varying linearly with the aluminium content. This result suggests that the acidity of Pd/Al40-SBA is probably underestimated due to the formation of thick alumina particles on the surface of the silica pores, or eventually due to pore clogging associated to the alumina bulky particle formation at the pore mouth or at the external surface of silica grain. The IR spectra of adsorbed pyridine on the catalysts after evacuation at 250, 350 and 450 °C are taken in order to estimate the strength of the acidity (Fig. S6, ESI). The intensity of the bands associated to adsorbed pyridine rapidly decreases for all catalysts, indicating a low to moderate strength of the acid sites.

Complementary characterization of Pd phase is assessed by H_2-TPR (Fig. 6). No hydrogen consumption was observed in the 25-800 °C temperature range for SBA-15 and Alx-SBA-15 supports. The H_2-TPR profiles of the Pd/SBA as well as the materials containing 5 and 20 % of Al revealed the presence of two peaks at low temperatures which corresponds to the reduction of palladium oxide particles ~~[49,50].~~ It is well known that PdO reduces easily at low temperatures (below 200 °C) [11,16,20,49-51]. The H_2 consumption at lower temperature (70-73 °C) is associated with the reduction of PdO outside of the pores, and the one at higher temperature (88-92 °C) is due to the reduction of PdO inside the pores. The TPR profile of Pd/Al40-SBA exhibits only one peak at lower temperature (42 ^oC). Similar results were reported by Gage et al. [32] for Pd/SBA. This result confirms the location of the PdO NPs at the external surface / pore mouths of the support due to their weak interaction with the support [52,53]. The negative peak observed at 82 °C is likely due to the decomposition of PdH_x. The metallic Pd^0 particle adsorbs H atoms and PdH_x (α or β) phases can be formed (α phase

contains less H atoms than the β phase) at low temperature, and the hydride is decomposed into metal when temperature increases.

3.2 Catalyst properties for the transformation of m-cresol

Table 3 displays the conversion of m-cresol and product distribution obtained at 300 °C under atmospheric and high pressure (30 bar) at different contact time values to ensure a low level of conversion (close to 10%). In the case of Pd/Al5-SBA and Pd/Al20-SBA, due to their high activity under 30 bar, the lowest conversion obtained was around 20%. The product distribution varies significantly with the support composition regardless of the pressure used.

Under atmospheric pressure, for the Pd/SBA catalyst, the conversion of m-cresol leads to 3-methylcyclohexanone and toluene, the former being the main product (62%). The incorporation of 5 wt.% of Al into the structure of SBA-15 (Pd/Al5-SBA) significantly increases the selectivity toward toluene (77%) compared to the Pd/SBA catalyst. It is also observed the formation of phenol, o-cresol, and xylenols (2,5-dimethylphenol; 3,4-dimethylphenol; 3,5-dimethylphenol; 2,4-dimethylphenol). The o-cresol isomer is obtained through isomerization, while phenol and xylenols are produced by a disproportionation reaction, both reactions are known to be catalyzed by acid sites [10,54,55]. Unfortunately, p-cresol could not be detected in our chromatographic conditions since its retention time is about the same that the one of m-cresol, as already indicated in the experimental part. Nevertheless, both cresol isomers (ortho and para cresol) are expected to be obtained in equimolar quantities, as already reported [10]. Further increase in the aluminium content (Pd/Al20-SBA and Pd/Al40-SBA) significantly increases the selectivity to phenol, xylenols and o-cresol, whereas the selectivity to toluene strongly decreases (from 77% with Pd/Al5-SBA to 22% with Pd/Al40-SBA). In addition, 3-methylcyclohexanone is no longer detected with the catalysts containing 20 and 40 wt.% of Al.

When the pressure was increased, a strong effect on the product distribution was observed. Indeed, m-cyclohexanone was the main product under 30 bar, whereas toluene was only observed in trace amount. In addition, methylcyclohexane which was never detected under atmospheric pressure, was observed in large amounts under 30 bar, its selectivity being between 14 and 37 mol.% depending on the catalyst. In addition, products obtained by isomerization and disproportionation reactions under atmospheric pressure were suppressed at 30 bar.

The reactant can be hence converted into several pathways: the DDO route leading only to toluene, the HYD route leading to oxygenated (alcohol and ketone) and deoxygenated (methylcycloalkenes and methylcycloalkane) products, the ISOM route yielding cresol isomers and the DISP route leading to phenol and xylenol isomers. The influence of the Al content, and thus, their catalyst acidity on the total reaction rate and the rates calculated for each reaction pathway is reported in Table 4 and presented in Fig.7. The DDO reaction rate initially increased with the addition of 5 wt.% of Al (corresponding to 0.57 μmol m^{-2} as total acidity), it continuously decreased with the increase in acidity, i.e. the content of Al. This may be due to the accumulation of larger PdO NPs and the formation of alumina at external surface of SBA-15 with the consequent reduction in the number of Pd-acid sites interfaces that is responsible to promote the deoxygenation route. The HYD route only yielding 3-methylcyclohexanone under atmospheric pressure was inhibited when Al was added in the catalytic support. On the opposite, further increase in acidity is accompanied by the promotion of the side reactions, as clearly indicated by the increase in the isomerization and disproportionation reaction rates (Fig. 7). However, increasing the Al content leads to an increase in Lewis acidity while the Bronsted acidity remained constant (Table 2). This may suggest that isomerization and disproportionation reactions are mainly promoted by Lewis acid sites.

The increase of pressure promoted the activity of all catalysts, especially for Pd/Al5-SBA which was about 500 times more active under 30 bar compared to atmospheric pressure. Both HYD and DDO routes were improved by pressure, the HYD route in large extend, in accordance with results reported previously [56]. For example, in the case of Pd/Al5-SBA, the rate of DDO and HYD reactions increased 12-fold and 11,000-fold, respectively, with the increase of the pressure. Thus, under high pressure, the HYD route became predominant and the DDO route was negligible. The introduction of 5 wt.% of Al, corresponding to 0.57 µmol m^{-2} as total acidity, increased the rate of the HYD route. However, further increase in catalyst acidity led to the decrease in HYD rate, as can be seen in Fig. 7. This decrease may be explained by the change in the textural properties of catalysts (Table 1).

Based on our results, we don't observed also correlation between palladium dispersion and reactions rates (Fig. S7). In fact, the catalytic properties of Pd/Al-SBA solids can be explained by the involvement of several factors such as acidity, textural properties and palladium dispersion.

In addition, as highlighted in Fig. S8 (ESI), an increase of pressure allowed an increase of the stability of the Pd/Al-5SBA catalyst. The beneficial effect of pressure can be attributed to a lower content of coke deposition due to the presence of large amount of hydrogen species under high pressure.

3.3 Reaction mechanisms involved during the transformation of m-cresol over Pd/Al-SBA-15 catalysts

There is a consensus that bifunctional catalysts composed by a metal particle combined with an acidic or oxophilic support is required for the deoxygenation reaction of phenolic compounds that are representative of the lignin fraction of lignocellulosic biomass [8-19]. In this case, both the metal and the support nature play an important role. The results of our work

show that the control of reaction pathways in the transformation of m-cresol is affected by the support composition which can leads to a modification of both physico-chemical and textural properties accordingly with the literature [8,13,15,20,25]. Indeed, the presence of Al is known to increase the acidity of the catalyst, as illustrated in Table 2. In addition, our results indicated that a high content of Al led to a decrease of their specific surface area (Table 1), which is consistent with the decrease of the surface accessibility and the partial obstruction of the mesopores, especially for the support containing 40 wt.% of Al. Furthermore, the dispersion and location of the metal particles through the pore structure of the support can play an important role in the reaction pathways. An appropriate combination of metal and acid sites density seems to improve the performance of catalysts for deoxygenation. In addition, mesoporous structures, among them SBA-15, may contribute to avoid metal sintering during reaction and pore blockage by heavy products.

To explain the deoxygenation of m-cresol, it has been proposed the involvement of a common intermediate (3-methyl-3,5-cyclohexadienone) between two parallel routes, as shown in Scheme 1. Such instable intermediate can be obtained by tautomerization of m-cresol and it can react by two different pathways: hydrogenation of the C=C bonds resulting in 3-methylcyclohexanone (HYD route) or hydrogenation of the C=O bond leading to the formation of an unsaturated alcohol which dehydrates to toluene (DDO route). Such mechanism has already been proposed by several authors [57-59].

In this work, under atmospheric pressure, the ketone was the only product formed by the HYD route whereas this ketone was further converted to deoxygenated products (cycloalkenes and cycloalkane) under 30 bar by consecutive dehydration and hydrogenation steps. It was also highlighted that the catalyst support allows the control of the reaction pathways. Supports without acidic properties, such as SiO_2, promotes the ring hydrogenation pathway. Indeed, our results show that 3-methylcyclohexanone obtained by hydrogenation of aromatic ring is the

main product observed on Pd/SBA (Table 3), in accordance with results reported by Gage et al. when phenol was used as reactant [32]. This ketone was unreactive under atmospheric pressure but it can be converted into deoxygenated products (cycloalkenes and cycloalkane) under high pressure.

It is well known that the introduction of acid and/or oxophilic sites on the support significantly changes the contribution of each reaction pathway. The increase of Lewis acidity on the catalyst by introduction of a low quantity of Al (5 wt.%) promoted the deoxygenation pathways under both reaction conditions.

At atmospheric pressure, the addition of 5 wt.% of Al an increased the r_{DDO} whereas the the r_{HYD} strongly decreased, modifying significantly the product distribution. Indeed, the r_{DDO}/r_{HYD} ratio was close to 16 on Pd/Al5-SBA whereas it was equal to 0.6 on Pd/SBA. Thus, the presence of Lewis acid sites on the modified support (Al-SBA-15) favors the dehydration of the tautomer alcohol intermediate formed, leading to toluene rather than its hydrogenation. This fact could be explained by a strong adsorption of the oxygen atoms on the Lewis acid sites, favoring the C=O bond hydrogenation. Under high pressure (30 bar), the presence of 5 wt.% of Al increased both r_{DDO} and r_{HYD} values in about the same extend (between 5 to 7), probably due to a high coverage of H_2 on Pd particles [60]. The presence of Lewis acid sites due to the presence of Al favors the deoxygenation of intermediates (ketone and alcohol) into methylcyclohexenes and methylcyclohexane. It is important to note that under this reaction condition, hydrogenation of toluene toward methylcyclohexenes and methylcyclohexane does not occur. This fact is in line with the effect of the contact time on the distribution of products over Pd/Al5-SBA (Fig. S9, ESI), which indicates that methylcyclohexane was only obtained by the HYD route by consecutive reactions (dehydration followed hydrogenation) from methylcyclohexanone, toluene being only observed in traces whatever the W/F value.

Our results are in accordance with the literature. Previous reports regarding the performance of Pd-based catalysts on the HDO of compounds such as phenol and m-cresol under atmospheric pressure have shown that mainly the oxygenated product, methyl-cyclohexanone is formed over a Pd/SiO_2 catalyst while toluene is selectively produced over Pd supported on acidic and/or oxophilic materials [11,15,16,20]. To the best of our knowledge, no catalytic properties of Pd based catalysts were reported under high pressure under continuous conditions. Shivhare et al. [37] also investigated the role of acid sites in the HDO of anisole in liquid phase over Pt supported on SBA-15 and Al-functionalized SBA-15 catalysts. Agreeing with our results, the introduction of aluminium enhanced the yield to cyclohexane. Such result can be explained by the strong hydrogenation ability of Pt compared to Pd, favoring the hydrogenation of benzene into cyclohexane. A series of various Ni/Al-SBA15 catalysts with different Si/Al ratios (50, 60, 70 and 80) was tested for the HDO of dibenzofuran (DBF) in liquid phase [33]. The authors proposed that the HDO of DBF proceeds through the hydrogenation of the aromatic ring on Ni metallic sites followed by cleavage of C-O bonds involving dehydration reactions. In agreement with our results, oxygenated products were dominant over Ni/SBA15 catalyst, while the incorporation of aluminium into the Ni/SBA-15 resulted in an outstanding improvement in the selectivity to the deoxygenated product, bicyclohexane. Thus, our results clearly show the existence of an optimum content of Al in Al-modified SBA-15 support, which is close to 5 wt%, allowing hence to obtain a maximum selectivity to toluene under atmospheric pressure or methylcyclohexane at high pressure (30 bar).

Regarding the isomerization and disproportionation pathways observed under atmospheric pressure, an increase of catalyst acidity leads to an increase of both r_{ISOM} and r_{DISP} reaction rates, as indicated in Table 3. Indeed, both isomerization and disproportionation reactions are typically acid-catalyzed reactions [61]. Such reactions were already reported to occur by

parallel reaction routes from the transformation of both m-cresol on H-beta zeolite support [10] and 2-ethylphenol on alumina support [62]. However, these reactions occurred only at atmospheric pressure condition, suggesting that the presence of a high coverage of H_2 inhibit such reactions. Isomerization reaction produces the ortho- and para-cresol isomers, whereas disproportionation reaction leads to phenol and xylenol isomers (Scheme 1). As expected, the increase in acidity promotes the isomerization and disproportionation reaction pathways. Nevertheless, this increase is accompanied by a decrease in the rate of deoxygenation, as highlighted in Fig. 7.

4. Conclusions

This work reported the effect of Al content (0, 5, 20 and 40 wt. %) in mesoporous silica (SBA-15) supports on the performance of Pd-based catalysts for the HDO reaction of m-cresol in gas phase under atmospheric and high pressure (30 bar). At higher of Al loading, accumulation of Al_2O_3 particles clogging the pores was observed. For Al content lower than 40 wt.%, the aluminium phase distribution throughout SBA-15 silica pores slightly affected the PdO size and distribution, nanoparticles being mostly located inside the mesopores. On the contrary, Pd/Al40-SBA exhibited the majority of Pd particles onto the Al_2O_3 phases situated outside of the SBA-15 grains or at the pore mouths.

The activity and the product distribution were significantly changed with the insertion of Al over silica at both reaction conditions. The creation of acidic sites over the support, through the incorporation of 5 wt.% Al, strongly enhanced the selectivity to the deoxygenated product, toluene or methylcychohexane. The DDO deoxygenation route, leading to toluene, was the main pathway on this catalyst under atmospheric pressure whereas the HYD route, leading to 3-methylcyclohexanone and methylcyclohexane, was the main route under pressure (30 bar). Further increase in Al loading on the silica support promoted side reactions such as

isomerization and disproportionation under atmospheric pressure, which are acid-catalyzed reactions. Changes in selectivities were rationalized in terms of palladium aggregation level and support acidity. Therefore, the results obtained demonstrated that adjusting the metal/acid site balance in the Pd/Al-SBA-15 bifunctional catalysts is an efficient way to control product distribution and improve the yield to the deoxygenated compounds during the upgrading of bio-oils containing phenolic compounds.

Acknowledgements

Camila A. Teles thank Coordenacao de Aperfeicoamento de Pessoal de Nivel Superior (CAPES - CAPES−COFECUB program –88881.142911/2017-01). Camila A. Teles, Jean-Marc Clacens, and Frederic Richard also acknowledge financial support from the European Union (ERDF), “Region Nouvelle Aquitaine”. This work (Pyreodeox project) was financially supported by ANR (Agence Nationale de la Recherche). The authors would like to thank Jean-Francois Tahon for SAXS facility. The Chevreul Institute is aknowledged for its help in the development of this work through the ARCHI-CM project supported by the “Ministère de l’Enseignement Supérieur de la Recherche et de l’Innovation”, the region “Hauts-de-France”, the ERDF program of the European Union and the “Métropole Européenne de Lille. Fabio B. Noronha thanks the Fundação de Amparo à Pesquisa do Estado do Rio de Janeiro (FAPERJ – E-26/202.783/2017), Conselho Nacional de Desenvolvimento Científico e Tecnologico (CNPq - 303667/2018-4; 305046/2015-2; 302469/2020-6) and the French government through the Programme Investissement d’Avenir (I-SITE ULNE / ANR-16-IDEX-0004 ULNE) managed by the Agence Nationale de la Recherche, CNRS, Métropole Européen de Lille (MEL) and Region Hauts-de-France for the financial support to “CatBioInnov” Project.

REFERENCES

[1] D.E. Resasco, S.P. Crossley, Catal. Today 257 (2015) 185-199.

[2] Y. Luo, V.K. Guda, E.B. Hassan, P.H. Steele, B. Mitchell, F. Yu, Energy Convers. Manag. 112 (2016) 319-327.

[3] W. Jin, L. Pastor-Pérez, D. Shein, A. Sepúlveda-Escribano, S. Gu, T.R. Reina, ChemCatChem 11 (2019) 924-960.

[4] S. Kim, E.E. Kwon, Y.T. Kim, S. Jung, H.J. Kim, G.W. Huber, J. Lee, Green Chem. 21 (2019) 3715-2743.

[5] P.M. Yeletsky, R.G. Kukushkin, V.A. Yakovlev, B.H. Chen, Fuel, 278 (2020) 118255.

[6] C. Li, X. Zhao, A. Wang, G.W. Huber, T. Zhang, Chem. Rev. 115 (2015) 11559-11624.

[7] G.W. Huber, S. Iborra, A. Corma, Chem. Ver. 106 (2006) 4044-4098.

[8] A. Foster, T.M.P. Do, R.F. Lobo, Top. Catal. 55 (2012) 118-128.

[9] H. Wan, R.V. Chaudhari, B. Subramaniam, Top. Catal. 55 (2012) 129-139.

[10] X. Zhu, L. Nie, L.L Lobban, R.G. Mallinson, D.E. Resasco, Energy Fuels 28 (2014) 4104-4111.

[11] C.A. Teles, R.C. Rabelo-Neto, J.R. Lima, L.V. Mattos, D.E. Resasco, F.B. Noronha, Catal. Lett. 146 (2016) 1848-1857.

[12] Q. Tan, G. Wang, L. Nie, A. Dinse, C. Buda, J. Shabaker, D.E. Resasco, ACS Catal. 5 (2015) 6271-6283.

[13] M.B. Griffin, G.A. Ferguson, D.A. Ruddy, M.J. Biddy, G.T. Beckham, J.A. Schaidle, ACS Catal. 6 (2016) 2715-2727.

[14] L. Nie, P.M. de Souza, F.B. Noronha, W. An, T. Sooknoi, D.E. Resasco, J. Mol. Catal. A: Chem. 388-389 (2014) 47-55.

[15] P.M. de Souza, R.C. Rabelo-Neto, L.E.P. Borges, G. Jacobs, B.H. Davis, T. Sooknoi, D.E. Resasco, F.B. Noronha, ACS Catal. 5 (2015) 1318-1329.

[16] C.A. Teles, R.C. Rabelo-Neto, G. Jacobs, B.H. Davis, D.E. Resasco, F.B. Noronha, ChemCatChem. 9 (2017) 2850-2863.

[17] A. Robinson, G.A. Ferguson, J.R. Gallagher, S. Cheah, G.T. Beckham, J.A. Schaidle, J.E. Hensley, J.W. Medlin, ACS Catal. 6 (2016) 4356-4368.

[18] I.T. Ghampson, C. Sepúlveda, A.B. Dongil, G. Pecchi, R. Garcia, J.L.G. Fierro, N. Escalona, Catal. Sci. Tech. 6 (2016) 7289-7306.

[19] A.J.R. Hensley, Y. Wang, J-C. McEwen, ACS Catal. 5 (2015) 523-536.

[20] C.A. Teles, P.M. De-Souza, R.C. Rabelo-Neto, M.B. Griffin, C. Mukarakate, K.A. Orton, D.E Resasco, F.B. Noronha, App. Catal. B: Environm. 238 (2018) 38-50.

[21] W. Song, Y. Liu, E. Barath, C. Zhao, J.A. Lercher, Green Chem. 17 (2015) 1204-1218.

[22] T. Prasomsri, M. Shetty, K. Murugappan, Y.R. Leshkov, Energy Environ. Sci. 7 (2014) 2660-2669.

[23] H. Fang, J. Zheng, X. Luo, J. Du, A. Roldan, S. Leoni, Y. Yuan, App. Catal. A: Gen. 529 (2017) 20-3.

[24] D. Gao, Y. Xiao, A. Varma, Ind. Eng. Chem. Res. 54 (2015) 10638-10644.

[25] P.M. Mortensen, J-D. Grunwaldt, P.A. Jensen, A.D. Jensen, ACS Catal. 3 (2013) 1774-1785.

[26] R.R. Barton, M. Carrier, C. Segura, J.L.G. Fierro, S. Park, H.H Lamb, N. Escalona, S.W. Peretti, App. Catal. A: Gen. 562 (2018) 294-309.

[27] I.T Ghampson, R. Canales, N. Escalona, App. Catal. A: Gen. 549 (2018) 225-236.

[28] F. Yang, H. Wang, J. Han, Q. Ge, X. Zhu, Catal. Today 347 (2020) 79-86.

[29] M. Zanuttini, B.D. Costa, C. Querini, App. Catal. A: Gen. 482 (2014) 352-361.

[30] S. Lin, L. Shi, M.M.L.R. Carrott, P.J.M. Carrott, J. Rocha, M.R. Li, X.D. Zou, Microporous Mesoporous Mater. 142 (2011) 526-534.

[31] A. Berenguer, T.M. Sankaranarayanan, G. Gomez, I. Moreno, J.M. Coronado, P. Pizarro, D.P. Serrano, Green. Chem. 18 (2016) 1938-1951.

[32] S.H. Gage, J. Engelhardt, M.J. Menart, C. Ngo, G.J. Leong, Y. Ji, B.G. Trewyn, S. Pylypenko, R.M. Richards, ACS Omega 3 (2018) 7681-7691.

[33] S. Gbadamasi, T.H. Ali, L.H.Voon, A.Y. Atta, P. Sudarsanam, S.K. Bhargava, S.B.A. Hamid, RSC Adv. 6 (2016) 25992-26002.

[34] M.J. Yu, S.H. Park, J-K. Jeon, C. Ryu, J.M. Sohn, S.C. Kim, Y-K. Park, J. Nano Sci. Techn. 15 (2015) 527-531.

[35] X. Li, J. Zhang, B. Liu, J. Liu, C. Wang, G. Chen, Fuel 243 (2019) 314-321.

[36] X. Li, L. Chein, G. Chen, J. Zhang, J. Liu, Renew. Energy 149 (2020) 609-616.

[37] A. Shivhare, J.A. Hunns, L.J. Durndell, C.M.A. Parlett, M.A. Isaacs, A.F. Lee, K. Wilson, ChemSusChem 13 (2020) 4945-4953.

[38] A. Ungureanu, B. Dragoi, V. Hulea, T. Cacciaguerra, D. Meloni, V. Solinas, E. Dumitriu, Microporous Mesoporous Mater. 163 (2012) 51–64.

[39] I. Mazilu, C. Ciotonea, A. Chirieac, B. Dragoi, C. Catrinescu, A.Ungureanu, S. Petit, S. Royer, E. Dumitriu, Microporous Mesoporous Mater. 241 (2017) 326-337.

[40] J. Liu, F. Qin, Z. Huang, L. Huang, Z. Liao, H. Xu, W. Shen, Catal. Letters 149 (2019) 1894-1902.

[41] B. Dragoi, E. Dumitriu, C. Guimon, A. Auroux, Microporous Mesoporous Mater. 121 (2009) 7-17.

[42] J-F. Dechézelles, C. Ciotonea, C. Catrinescu, A. Ungureanu, S. Royer, V. Nardello-Rataj, Langmuir 36 (2020) 3212-3220.

[43] J. Wang, Q. Liu, Solid State Commun. 148 (2008) 529-533.

[44] A. Chirieac, B. Dragoi, A. Ungureanu, C. Ciotonea, I. Mazilu, S. Royer, A.S. Mamede, E. Rombi, I. Ferino, E. Dumitriu, J. Catal. 339 (2016) 270-283.

[45] C.A. Emeis, J. Catal. 141(1993) 347.

[46] Y. Li, W. Zhang, L. Zhang, Q. Yang, Z. Wei, Z. Feng, C. Li, J. Phys. Chem. B 108 (2004) 9739-9744.

[47] A.J.J. Koekkoek, J.A.R. Veen, P.B. Gerrtisen, P. Giltay, P.C.M.M. Magusin, E.J.M. Hensen, Microporous Mesoporous Mat. 151 (2012) 34-43.

[48] M. Lindo, A.J. Vizcaíno, J.A. Calles, A. Carrero, Int. J. Hydrog. Energy 35 (2010) 5895-5901.

[49] C.A. Teles, R.C. Rabelo-Neto, N. Duong, J. Quiroz, P.H.C. Camargo, G. Jacobs, D.E. Resasco, F.B. Noronha, App. Catal. B: Environ. 277 (2020) 119238.

[50] R.R. Chada, S.S. Enumula, K.S. Koppadi, V.R.B. Gurran, S.R.R. Kamaraju, D.R. Burri, Chem. Select 3 (2018) 9946-9952.

[51] A.M. Barrios, C.A. Teles, P.M. De-Souza, R.C. Rabelo-Neto, G. Jacobs, B.H. Davis, L.E.P. Borges, F.B. Noronha, Catal. Today 302 (2018) 115-124.

[52] F.A. Lewis, Academic press, London-New York, 1967.

[53] F.B. Noronha, M. Schmal, M. Primet, R. Frety, Applied Catalysis 78 (1991) 125-139.

[54] G. Liu, Y. Zhao, J. Guo, Catalysts 6(2) (2016) 19.

[55] L. Nie, B. Peng, X. Zhu, ChemCatChem, 10 (2018) 1064-1074.

[56] V.O.O. Gonçalves, P.M. De-Souza, T. Cabioc'h, V.T da Silva, F.B. Noronha, F. Richard, Appl. Catal. B 219 (2017) 619-628.

[57] P.M. De-Souza, R.C. Rabelo-Neto, L.E.P. Borges, G. Jacobs, B.H. Davis, D.E. Resasco, F.B. Noronha, ACS Catal. 7 (2017) 2058-2073.

[58] C.A. Teles, P.M. De-Souza, A.H.Braga, R.C. Rabelo-Neto, A. Teran, G. Jacobs, D.E. Resasco, F.B. Noronha, App. Catal. B: Environ. 249 (2019) 292-305.

[59] V.O.O. Gonçalves, S. Brunet, F. Richard, Catal. Lett. 146 (2016) 1562-1573.

[60] D. Liu, G. Li, F. Yang, H. Wang, J. Han, X. Zhu, Q. Ge, J. Phys. Chem. C 121 (2017) 12249-12260.

[61] M. Javamani, C.N. Pillai, J. Catal. 82 (1983) 485-488.

[62] Y. Romero, F. Richard, S. Brunet, App. Catal. B: Environ. 98, 3-4 (2010) 213-223.

Table 1. Elemental composition, structural and textural properties of the PdO-based catalysts.

Catalyst	wt.% Al[a]	wt.% Pd[a]	S_{BET}[b] (m^2 g^{-1})	S_{micro}[c] (m^2 g^{-1})	V_p[d] (m^3 g^{-1})	V_{micro}[e] (m^3 g^{-1})	D_p[f] (nm)
Pd/SBA	-	1.7	539	75	1.07	0.03	7.2
Pd/Al5-SBA	4.5	1.7	377	75	0.78	0.03	7.3
Pd/Al20-SBA	20.5	1.9	378	68	0.80	0.03	7.1
Pd/Al40-SBA	43.8	2.0	279	49	0.49	0.02	6.0

[a] Aluminium or Palladium loading (wt.%) from ICP-EOS analysis; [b] BET surface area; [c] Micropore surface area; [d] Total pore volume; [e] Micropore volume; [f] BJH pore diameter calculated from the desorption branch.

Table 2. Palladium oxide dispersion / size and acidic properties for Pd-O based catalysts.

Sample	d^a (nm)	D^b (%)	d^c (nm)	Total acidity ($\mu mol\ g^{-1}$)	Total acidity ($\mu mol\ m^{-2}$)	Acid sites distribution ($\mu mol\ g^{-1}$)		Acid sites distribution ($\mu mol\ m^{-2}$)	
						Bronsted	Lewis	Bronsted	Lewis
Pd/SBA	3.4	47	2.4	0.0	0.00	0	0	0.00	0.00
Pd/Al5-SBA	2.9	47	2.4	214	0.57	35	178	0.09	0.47
Pd/Al20-SBA	2.4	61	1.8	269	0.71	35	234	0.09	0.62
Pd/Al40-SBA	3.1	38	3.4	273	0.98	33	240	0.11	0.86

[a] PdO particle size calculated by TEM (ImageJ software); [b] Pd dispersion estimated by H_2 chemisorption; [c] Pd particle size calculated on the basis of H_2 chemisorption dispersion.

Table 3. Product distribution for the transformation of m-cresol over the Pd based-catalysts ($T_{reduction}$ = 573 K, $T_{reaction}$ = 573 K, 1 h of TOS). Standard deviation of experimental values close to 5%.

Reaction pressure (bar)	Catalyst	W/F (g h mol^{-1})	Conversion (%)	Selectivity (%)							
					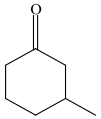	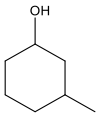		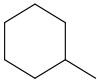	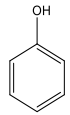	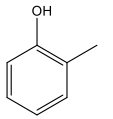	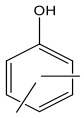
1	Pd/SBA	70	7	38	62	-	-	-	-	-	-
	Pd/Al5-SBA	81	5	77	5	-	-	-	3	9	6
	Pd/Al20-SBA	94	6	50	-	-	-	-	8	27	15
	Pd/Al40-SBA	94	5	22	-	-	-	-	14	46	18
30	Pd/SBA	1.0	6	1	80	3	2	14	-	-	-
	Pd/Al5-SBA	1.0	29	2	64	1	3	30	-	-	-
	Pd/Al20-SBA	0.9	21	1	57	1	4	37	-	-	-
	Pd/Al40-SBA	1.1	11	1	64	2	6	27	-	-	-

Table 4. Calculated reaction rates (in mmol g^{-1} h^{-1}) for the conversion of m-cresol and the different reaction pathways proposed for the transformation of m-cresol over Pd-based catalysts. Standard deviation of experimental values close to 5%.

Reaction pressure (bar)	Catalyst	r_{TOT}	r_{DDO}	r_{HYD}	r_{ISOM}	r_{DISP}
1	Pd/SBA	1.06	0.40	0.66	0.00	0.00
	Pd/Al5-SBA	0.62	0.48	0.03	0.06	0.05
	Pd/Al20-SBA	0.60	0.30	0.00	0.16	0.14
	Pd/Al40-SBA	0.55	0.12	0.00	0.25	0.18
30	Pd/SBA	61.8	0.8	61.0	-	-
	Pd/Al5-SBA	332.0	5.8	326.2	-	-
	Pd/Al20-SBA	240.4	3.6	236.8	-	-
	Pd/Al40-SBA	105.0	1.5	103.5	-	-

Figure 1. (a) SAXS patterns and (b) X-ray diffraction patterns at high angle of the silica supported PdO catalysts. ICCD file 88-2434: PdO.

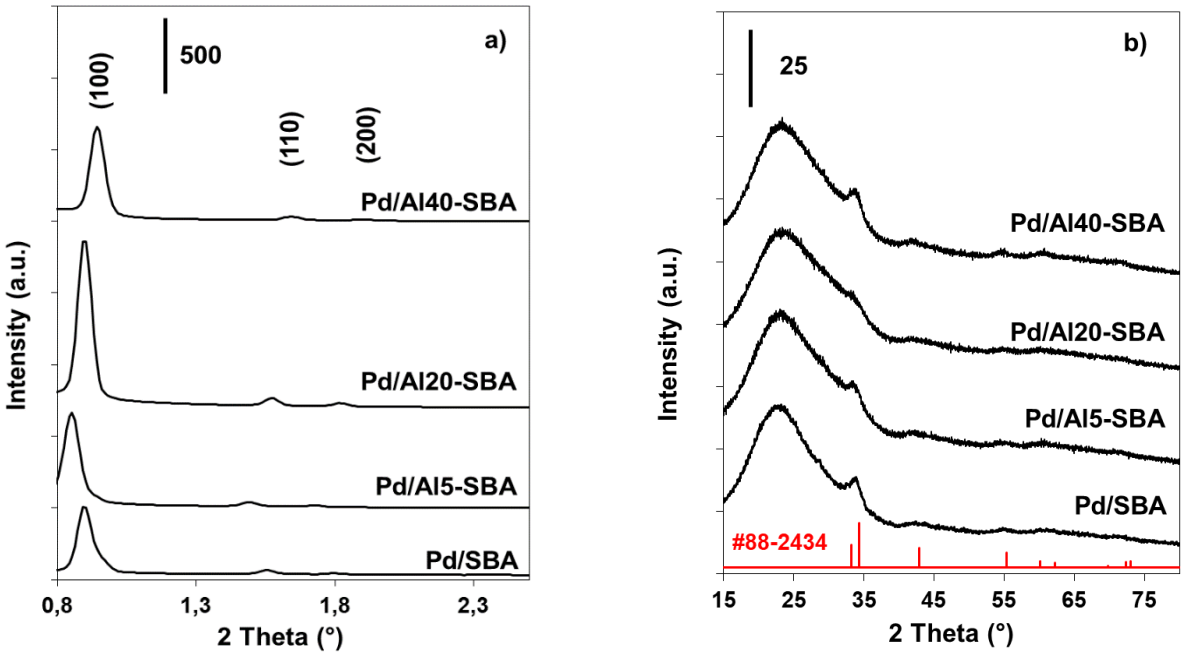

Figure 2. (a) N_2 adsorption-desorption isotherms and (b) B.J.H. pore size distribution obtained for PdO based-catalysts.

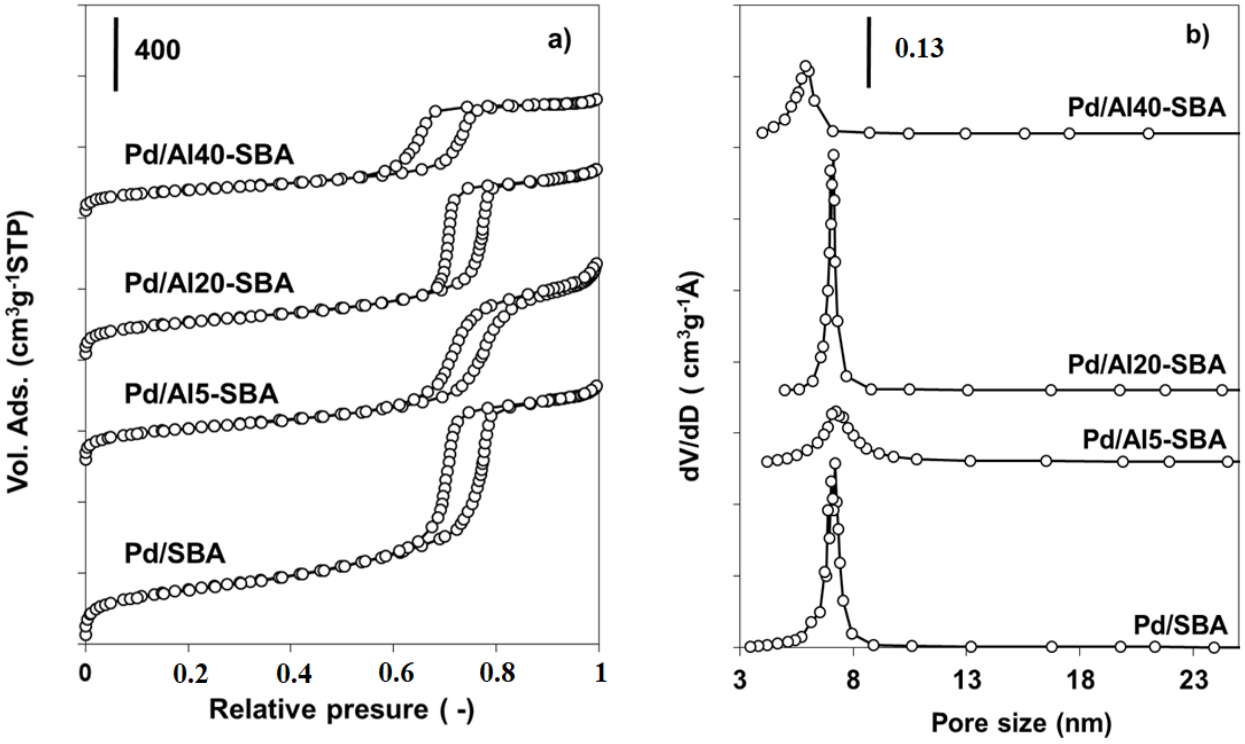

Figure 3. Representative HAADF images of the PdO-based catalysts.

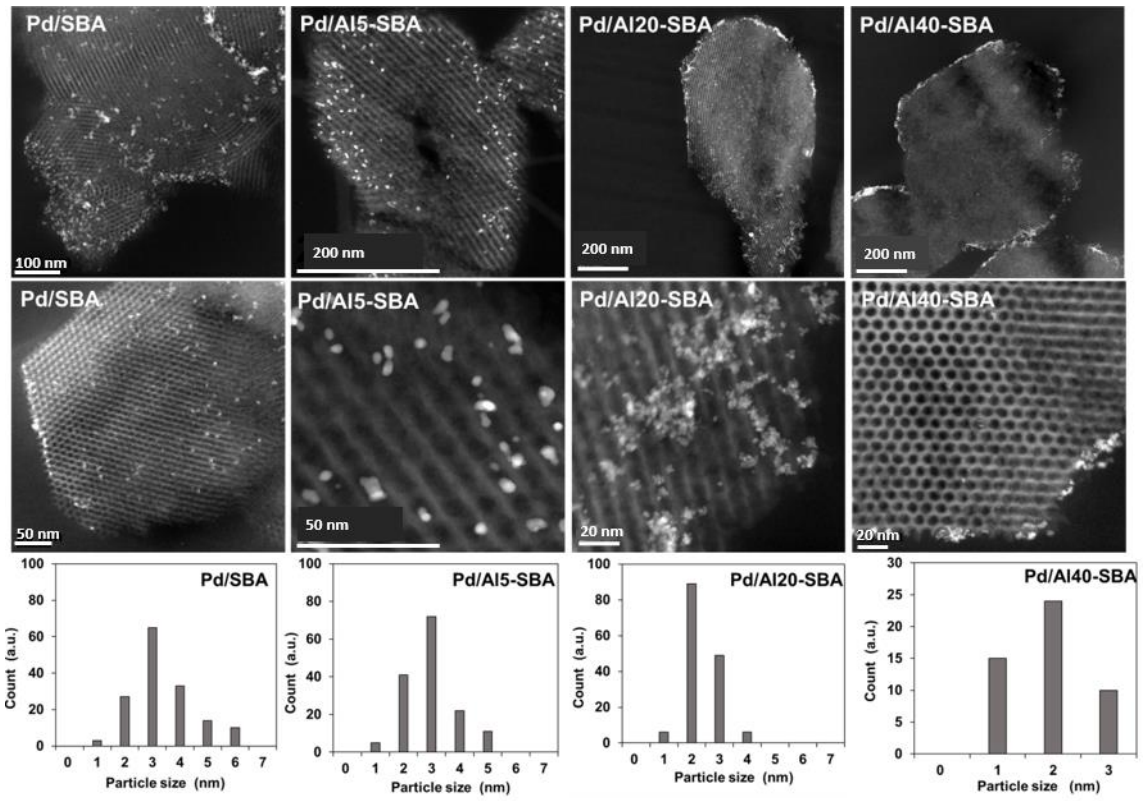

Figure 4. (a,b,c) Representative HAADF images, (d,e,f) palladium EDX elemental maps, (g,h,i) aluminium STEM-EDX mapping analysis obtained for PdO-based catalysts.

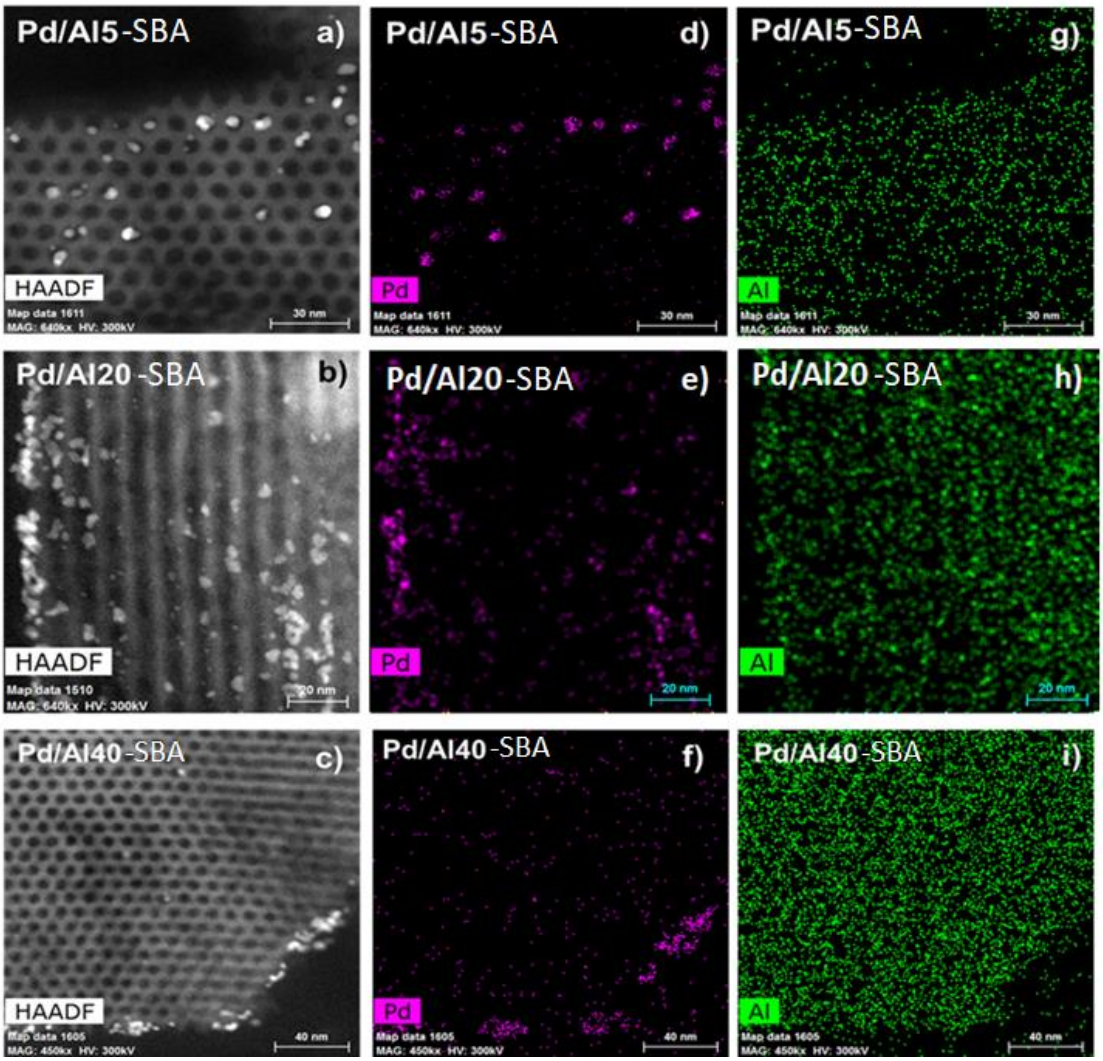

Figure 5. IR spectra of adsorbed pyridine after outgassing at 150 °C, obtained for PdO-based-catalysts. B: Brønted; L: Lewis.

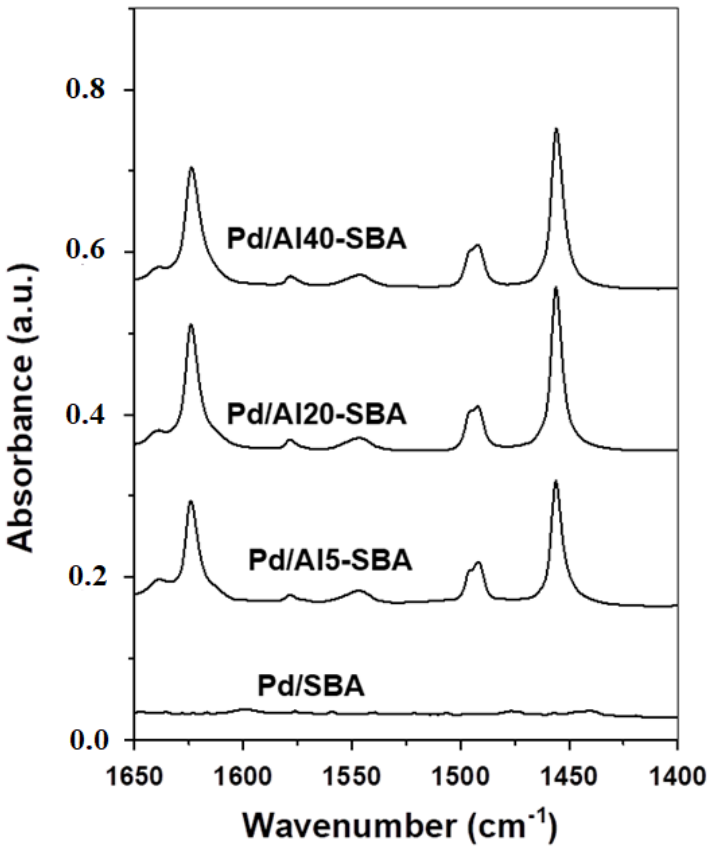

Figure 6. H_2-TPR profiles recorded for PdO-based catalysts.

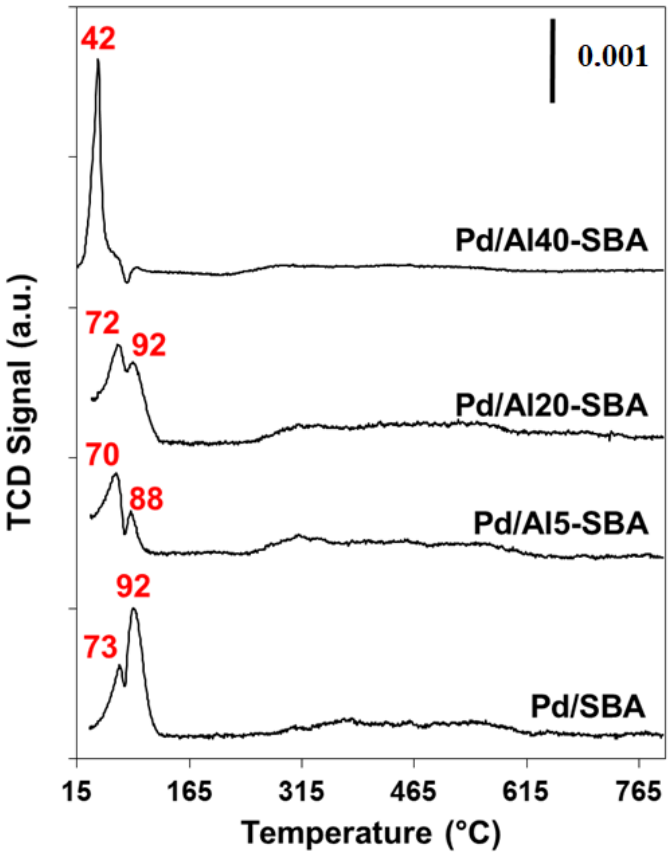

Figure 7. Effect of the Al content on the reaction rates calculated for the transformation of m-cresol over Pd-based catalysts under atmospheric pressure (a) and 30 bar (b) (■) r_{TOT}: total rate (●) r_{DDO}: deoxygenation rate, (▲) r_{HYD}: hydrogenation rate, (◆) r_{ISOM}: isomerization rate, (■) r_{DISP}: disproportionation rate.

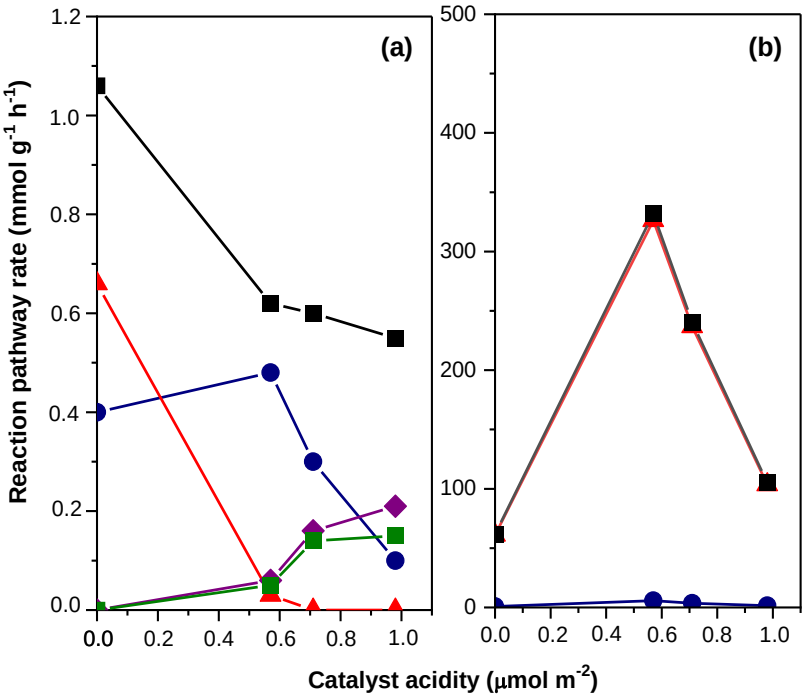

Scheme 1. Reaction pathways proposed for the transformation of m-cresol over Pd-based catalyst.

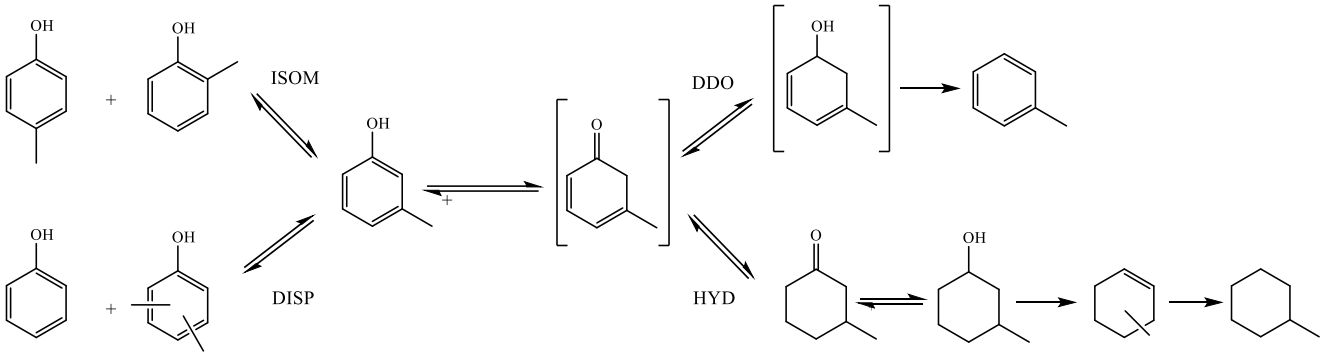

Highlights:

- The incorporation of Al on the SBA-15 structure is satisfying up to 20 wt.% of aluminium.
- Higher Al content leads to aggregation of PdO particles and formation of Al_2O_3 outside SBA-15.
- The product distribution is strongly affected by the incorporation of acid sites and by the pressure.
- Incorporation of 5 wt.% Al gives toluene as main product under atmospheric pressure and 3-methylcyclohexanone under 30 bar.